Carbon 182 (2021) 167–174

Contents lists available at ScienceDirect

Carbon

journal homepage: www.elsevier.com/locate/carbon

Design and mechanism of photocurrent-modulated graphene field-effect transistor for ultra-sensitive detection of DNA hybridization

Yang Sun [a, b], Shicai Xu [c], Tiying Zhu [a], Jiajun Lu [a], Shuo Chen [a], Maomao Liu [b], Guangcan Wang [a], Baoyuan Man [a, ***], Huamin Li [b, **], Cheng Yang [a, b, *]

[a] School of Physics and Electronics, Shandong Normal University, Jinan, 250014, People's Republic of China
[b] Department of Electrical Engineering, University at Buffalo North Campus, Buffalo, NY, 14260, USA
[c] Shandong Key Laboratory of Biophysics, Institute of Biophysics, Dezhou University, Dezhou, 253023, People's Republic of China

ARTICLE INFO

Article history:
Received 11 March 2021
Received in revised form
26 May 2021
Accepted 1 June 2021
Available online 5 June 2021

Keywords:
Photocurrent
Field-effect transistor
Graphene
DNA hybridization
Biosensor

ABSTRACT

Field-effect transistors (FET) using low-dimensional materials has attracted attention for detection of DNA hybridization. Here, we proposed a photocurrent-modulated FET sensor, where the $I_{photocurrent(gate)} + I_{photocurrent(DNA)}$ dramatically enhance the response signal, $I_{current}$, compared to a traditional FET sensor. The proposed sensor successfully detects DNA signals with a limit of detection (LOD) down to attomolar concentrations that is nearly 100x lower than a traditional FET sensor. The sensing mechanism is postulated and discussed. The results suggest that photo-coupled modulation opens new avenues for further development of the FET in biosensing applications.

1. Introduction

DNA carries a broad range of critical biological information and genetic instructions. It also supplies clues in the diagnosis and treatment for a range of diseases [1–4]. Therefore, designing a viable platform for collection and analysis of DNA information is highly desirable. Recently, the FET biosensor has emerged for rapid DNA detections due to its simple structure and label-free property [5–9]. Many diseases have been successfully detected and recognized using the FET sensor. Both Alzheimer's disease and Trisomy 21 syndrome were confirmed using the graphene-based FET sensor and the MoS_2-based FET sensor to detect DNA hybridization [10,11]. Binding kinetics and affinities of the DNA hybridization can also be calculated using the FET sensor [12]. One inherent limit for these FET sensors stems from the very small fraction of disease-related DNA in the body, and therefore further improvement of the limit of detection (LOD) for the FET sensor is important.

The present focus in sensor research has been testing configurations of probe DNA or channel materials for improving the sensitivity of FET sensor to DNA hybridization detection [13–18]. DNA possesses a gating effect and this is the main sensing mechanism for the traditional FET sensor to detect DNA hybridization [19–22]. These FET sensors have reached close to their theoretical LOD and only small improvements can be found during the manufacturing processes [23–25]. Finding new sensing mechanisms to significantly enhance the FET sensors' sensitivity for DNA hybridization detection remains a key approach for advancement.

Herein we propose a photocurrent-modulated FET sensor for detection. Initially unrecognized DNA signals were detected after the sensor was modulated by photo-generated current. The modulation mechanisms are based on (1) the gating effect-dependent band profile of the graphene on the channel and (2) the gating effect-independent band profile of the graphene on the electrodes. These effects are qualitatively discussed below. The photocurrent-modulated FET shows remarkable DNA detection capabilities with an LOD close to 1 aM, which is nearly 100 times lower than a similar traditional FET sensor.

* Corresponding author. School of Physics and Electronics, Shandong Normal University, Jinan, 250014, People's Republic of China.
** Corresponding author.
*** Corresponding author.
E-mail addresses: byman@sdnu.edu.cn (B. Man), huaminli@buffalo.edu (H. Li), chengyang@sdnu.edu.cn (C. Yang).

https://doi.org/10.1016/j.carbon.2021.06.003
0008-6223/

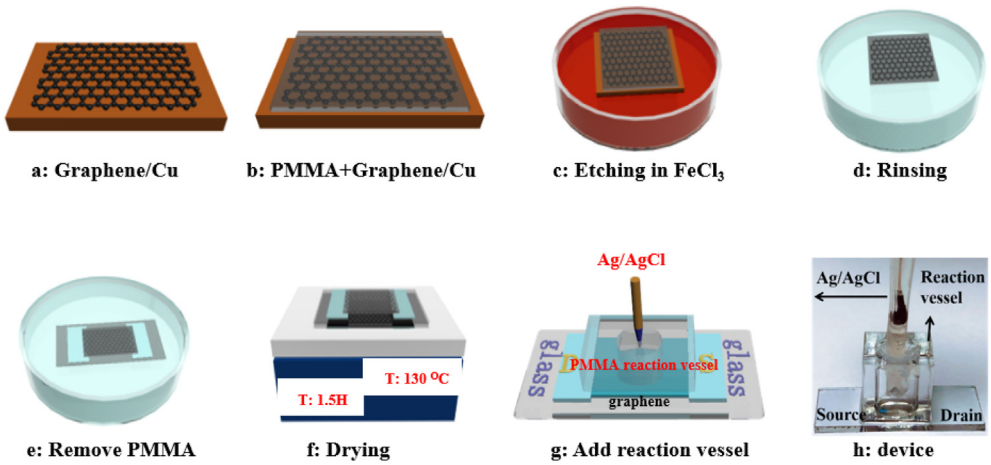

Fig. 1. (a) Cu + Graphene. (b) Cu + Graphene + PMMA. (c) Copper foil etched in ferric chlo-ride solution. (d) Graphene + PMMA rinsed with DI water. (e) PMMA was removed and washed with acetone, ethanol, and deionized water. (f) The graphene FET dried 1 h. (g) PMMA reaction vessel mounted on the FET. (h) Photograph of the FET sensor. (A colour version of this figure can be viewed online.)

2. Experimental section

2.1. Materials

Double-layer graphene was obtained using a chemical vapor deposition (CVD) system. Copper foil (thickness 250 μm; purity 99.99%) cleaned by HCl/H_2O (1:20) was used as the substrate for graphene growth. Methane and Hydrogen gas were used as the carbon source and auxiliary gas. The ITO/SiO_2 substrate was purchased from GULUO GLASS (Luo yang) Co., Ltd. 1-Pyrenebutanoic acid succinimidyl ester (PBASE), PBS (pH = 7.0–7.2; 137 mM NaCl), ethanolamine and *N*,N-dimethylformamide (DMF) were purchased from Aladdin Co., Ltd. The sequence of different type DNA purchased from Sangon Biotech (shanghai) Co., Ltd is shown in

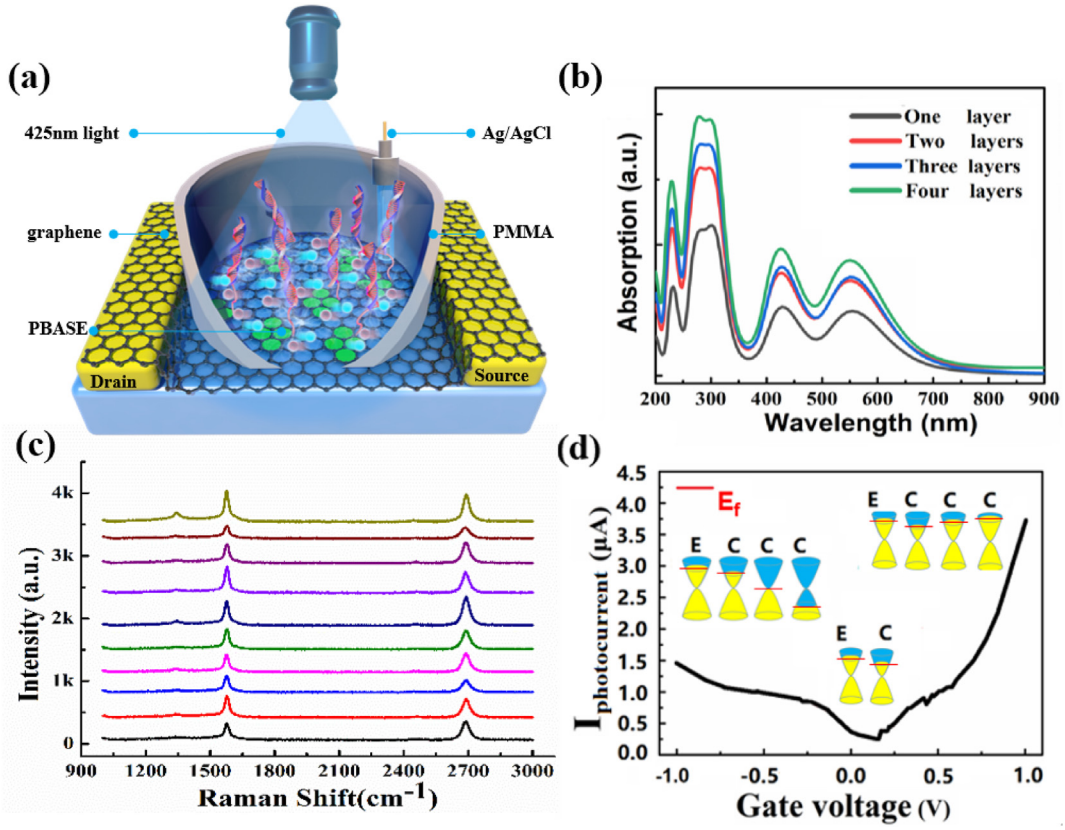

Fig. 2. (a) Schematic illustration of photocurrent-modulated FET sensor. (b) Light absorption of graphene. (c) Raman spectrum of double-layer graphene. (d) Photocurrent of the proposed FET sensor that bound with DNA. E: electrode; C: channel; Power of light is 6 W; $V_{SD} = 0.1V$. (A colour version of this figure can be viewed online.)

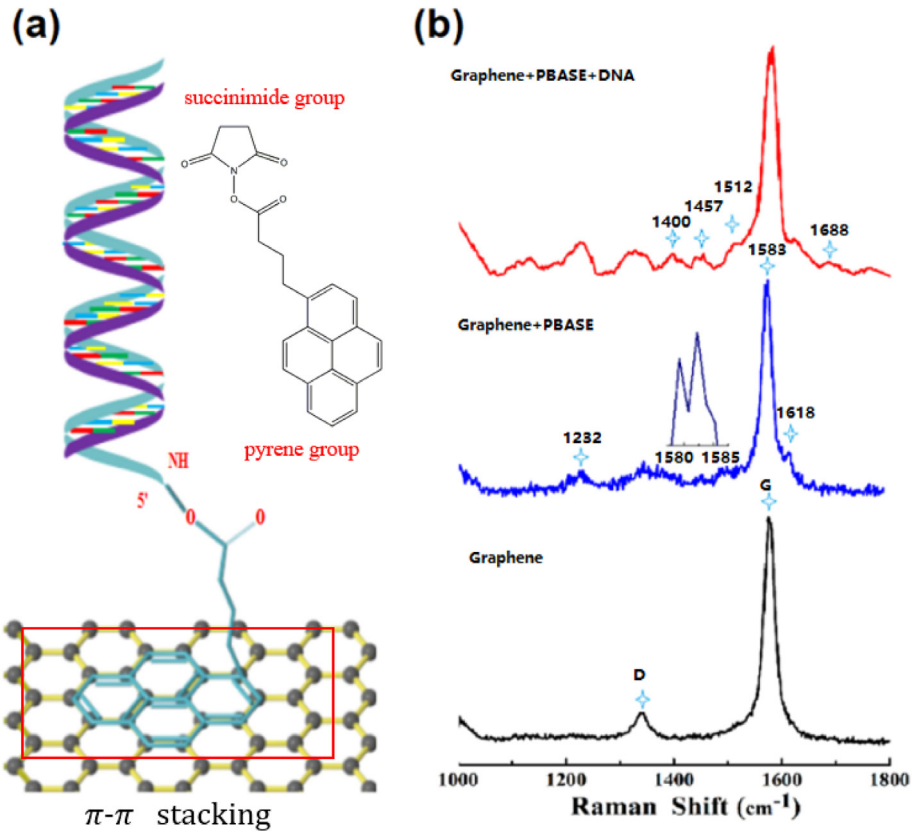

Fig. 3. (a) The mechanism of PBASE works as linker. The insert is PBASE model (b) Raman characterization of PBASE functionalize graphene and immobilize DNA.

supplementary materials table S1.

2.2. Fabrication of the FET sensor

CVD graphene on the Cu substrate is shown in Fig. 1a. PMMA was used as the support layer to transfer the graphene from the Cu substrate to ITO/SiO_2 substrate by etching the Cu substrate in $FeCl_3$ solution (27 g/100 mL), as shown in Fig. 1b and c. ITO was used as a source and drain for the FET devices. Graphene/PMMA was rinsed 3 times with deionized water for 10 min to remove $FeCl_3$ and $CuCl_2$, as shown in Fig. 1d. The PMMA/graphene was sequentially immersed in acetone, ethanol and deionized water for 30 min each to remove PMMA, as shown in Fig. 1e. This scheme progressively removes the PMMA, acetone, and ethanol moving to hydrophilic DI water. Finally, the home-made PMMA reaction vessel was mounted on the FET with UV curable adhesive and a AgCl reference electrode was placed above the channel for the gate voltage (V_G), as shown in Fig. 1f and g. Fig. 1h shows a photograph of the fabricated liquid gated - graphene FET sensor. Light with wavelength of 425 nm and power of 6 W was selected as the light source.

2.3. Functionalization and immobilization

PBASE was dissolved in DMF and was used as the linker between the graphene and probe DNA. First, 10 mM PBASE solution was added into the reaction vessel to react with graphene for 6 h. Next, DMF removed the excess PBASE. Then 1 μM DNA probe, whose 5′ was modified with amino, was dropped onto the surface of the sensing material and was reacted with PBASE for 16 h. The unbound probe DNA was washed away by phosphate buffer. Finally, 100 mM ethanolamine was used to deactivate the excess reactive groups of PBASE and prevent nonspecific binding events.

2.4. Characterization

The transfer characteristics of photocurrent-modulated FET were recorded by semiconductor parameter analyzer (Keithiey 4200). The thickness and uniformity of the graphene films were characterized by Raman spectroscopy (Horiba HR-800).

3. Result and discussion

3.1. Properties of DNA biosensor

The sensor effectively generates photocurrent to modulate the original current signal and enhance the sensitivity of the traditional FET sensor. The photocurrent-modulated FET sensor consists of graphene as the channel material, PMMA unit as the reaction vessel, ITO films as the source/drain electrode, Ag/AgCl as the gate electrode and the light source has a wavelength of 425 nm, as shown in Fig. 2a. The optimal conditions that graphene layers and light wavelength for the proposed sensor were explored by the Vienna Ab-initio Simulation Package simulation (VASP) [26]. Detailed simulation parameters were shown in Supplementary materials Simulation. Fig. 2b shows the simulation results that graphene has the highest light absorption intensity with wavelength around 300 nm and the second and third highest light absorption intensity with wavelength around 425 nm and 550 nm. Due to the light around 300 nm has destructive effect of DNA according to Refs. [27,28], the light with wavelength 425 nm was used as the light source for the photocurrent-modulated FET sensor. The intensity of absorption increased with the number of graphene

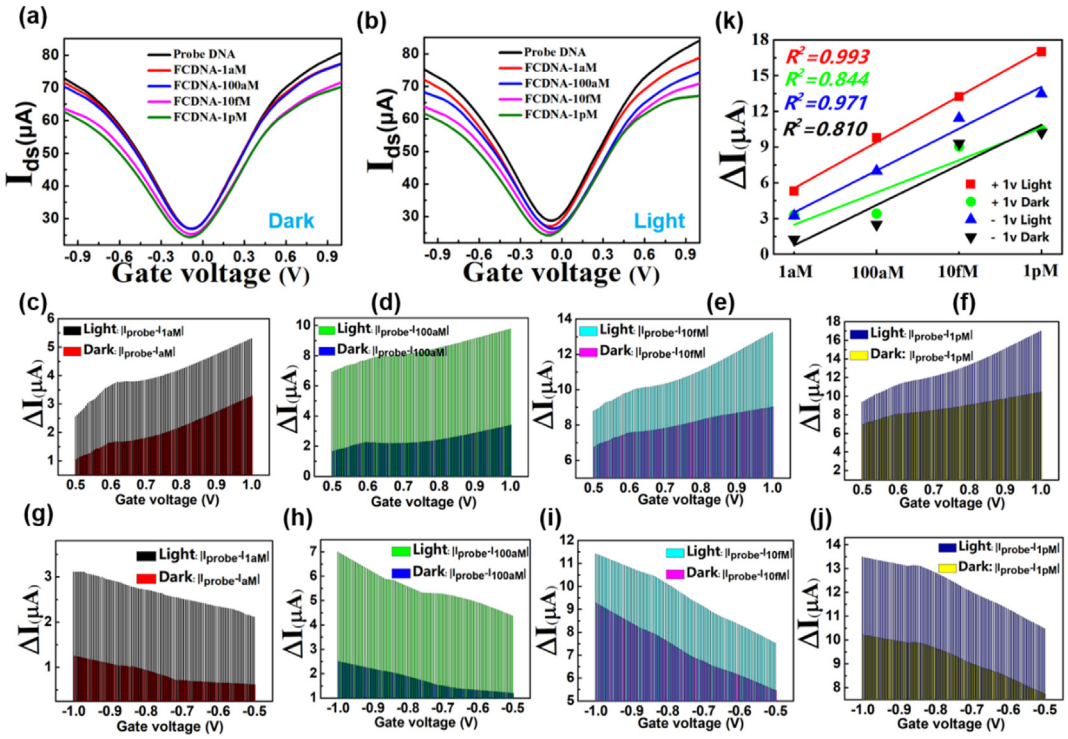

Fig. 4. (a)Transfer characteristics of the traditional FET sensor for DNA hybridization detection. (b)Transfer characteristics of the photocurrent-modulated FET sensor for DNA hybridization detection. (c–f) and (g–j) Comparisons of signal intensity that obtained by the traditional FET sensor or the photocurrent-modulation FET sensor to detect DNA hybridization in the same concentration, respectively. (k) Comparison of signal linearity that obtained by the traditional FET sensor or the photocurrent-modulation FET sensor. $\Delta I = \left|I_{probe} - I_{FCDNA}\right|$. (A colour version of this figure can be viewed online.)

layers at the wavelength 425 nm and 1–2 layers graphene can be stably growth in our Lab, so, double-layer graphene was chosen as the sensing material for our photocurrent-modulated FET sensor. As shown in Fig. 2c, the Raman spectrum of graphene clearly shows that the ratio of peak intensity of 2D/G is close to 1 and this result is also confirmed by Raman mapping as shown in Supplementary information Note 1. This ratio supports the formation of graphene with double layers [29]. Fig. 2d shows that the proposed FET sensor effectively generates a photocurrent and is dramatically tuned by the gating effect which depends on both the gate voltage (V_G) and the negative charged DNA (V_{DNA}). The formation of the energy barrier between the graphene on the channel and the graphene on the electrode is critical to generate a photocurrent as shown in the inserts of Fig. 2d. It has been established that the Fermi level of bilayer graphene is mainly modulated by gate-induced carrier density, n, as Equation (1) [30,31] :

$$E_F = \frac{\hbar^2 \pi n}{2m^*} \tag{1}$$

$\hbar$ is the reduced Planck constant. m* is the effective electron mass, for a specific sensor, m*is a constant. Gate-induced carrier density, n, is defined as equation (2) [30]:

$$\mathrm{n} = \frac{C_g}{q}(V_G - V_{\mathrm{CNP}}) \tag{2}$$

where $C_g$is the gate capacitance per unit area, for this sensor C_g equal to $2Fm^{-2}$and the calculation process of C_g is shown in supplementary information Note 2. Without bound DNA, the n is mainly tuned by the gate voltage. The formation of energy barrier to contribute photo-induced carrier density n' is depend on gate voltage. For the sensor bound with DNA, in addition to gate voltage (V_g), n is also tuned by negative charged DNA (V_{DNA}). Therefore, Equation (2) is changed to Equation (3):

$$\mathrm{n} = \frac{C_g}{q}\left(V_{gate\ voltage} + V_{DNA} - V_{\mathrm{CNP}}\right) \tag{3}$$

Equations (1) and (3) show that DNA plays an important role in modulating Fermi level and energy barrier. Here, the formation of energy barrier to contribute photo-induced carrier density n' is both depend on gate voltage and negative charged DNA. It has been established that the photocurrent arises from photo-induced carriers related by Equation (4) [32] :

$$I_{photocurrent} = q\mu n' \mathrm{EWD} \tag{4}$$

That suggests gradient DNA concentrations with different V_{DNA} can generate photocurrents to different degrees to modulated the original current signal.

3.2. Functionalization and hybridization of DNA biosensor

PBASE was selected to perform the functionalization of graphene and the immobilization of DNA. As shown in Fig. 3a, PBASE bind graphene by stacking of its pyrene group onto the graphene surface and immobilize the DNA by the conjugation reaction between the amine group of the probe DNA and the amine-reactive succinimide group of PBASE. In order to avoid nonspecific absorption, ethanolamine was used as the blocking agent to inactivate the excess part of PBASE. As shown in Fig. 3b, all the main fingerprint peaks of DNA and PBASE were obtained and these peaks can be clearly distinguished, which indicates that the process of functionalization and immobilization was successfully realized. The peaks at 1232 cm^{-1}, 1583 cm^{-1} and 1618 cm^{-1} can be assigned to

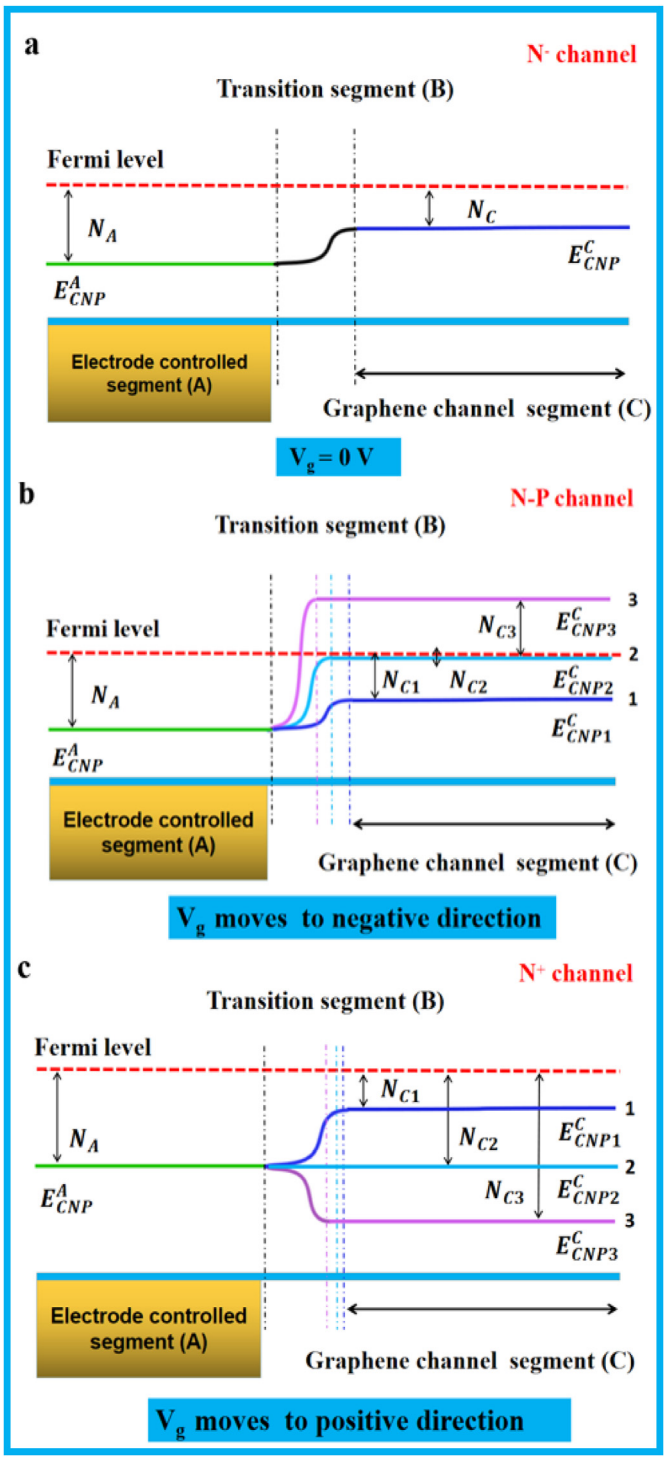

Fig. 5. Sensing mechanism model: the band profile of the graphene on channel and that of the graphene on electrodes under various gate voltage. (A colour version of this figure can be viewed online.)

the pyrene group resonance, which effectively proved that PBASE had attached onto the graphene surface. The peak at 1688 cm^{-1} was caused by the introduction of amino, which suggests that the Probe DNA was successfully bound to graphene. Other peaks can be assigned to the modes of DNA as described in our previous works [12,25].

3.3. Sensitivity of the photocurrent-modulated FET sensor

Response signal changes from $I_{current}$ to $I_{current} + I_{photocurrent(gate\ voltage)} + I_{photocurrent(DNA)}$. The change intensity of the response signals between the lowest concentration and the highest concentration is about 3–4 times in our manuscript, which are highly consistent with the published papers [16,25,33]. Transfer characteristics curve of the FET sensor to detect DNA hybridization with the optical source on and off were compared to show the importance of $I_{photocurrent(gate)} + I_{photocurrent(DNA)}$. Fig. 4a shows the traditional FET sensor cannot detect DNA signals with very low concentrations (from 1 aM to 1 pM). In Fig. 4b, the response signal shows significant visible changes after photocurrent modulation, especially under high gate voltages ($\pm 0.5V - \pm 1V$). Comparing Fig. 4a and b, it is clear that these Dirac points were separated significantly than before, after photocurrent modulation. However, there still no obvious regularly change. The reason is that the photocurrent only has a large generation under high gate voltage range ($\pm 0.5V - \pm 1V$), and is very weak under the low gate voltage range ($-0.5V - 0.5V$), especially near Dirac point, as shown in Fig. 2d. Dirac point may change regularly with higher photocurrent depending more suitable light power and we will further discuss and research that in the further. With the present photocurrent, the signal of gradient DNA in the high gate voltage range ($\pm 0.5V - \pm 1V$) changes regularly and can be clearly distinguished, which is enough to work as an effective marker-signal of DNA detection. In this study, we only focus on the regular separation of the DNA signals with gradient concentrations under the high gate voltage range, and do not pay attention to the signals under the low gate voltage range. Fig. 4c–f and Fig. 4h–j compare the response signals obtained by traditional FET sensor and photocurrent-modulated FET sensor at a gate voltage range from $\pm 0.5V$ to $\pm 1V$. These results clearly show that in detecting DNA hybridization at any concentration, the photocurrent-modulated FET sensor generates a larger response signal than the traditional FET sensor. The response signal of the sensor increases with gate voltage and DNA concentration. Obviously, photocurre $I_{photocurrent(gate\ voltage)} + I_{photocurrent(DNA)}$ played an important role in enhancing the weak detection signal. LOD close to 1 aM suggests that obtained FET sensor present higher sensitivity compared to the published works as shown in table S1. Moreover, the signal linearity of the photocurrent-modulated FET sensor and the traditional FET sensor for detecting DNA hybridization at gate voltage $\pm 1V$ was compared. The results show that photocurrent-modulated FET sensor exhibits good linear response to DNA hybridization in the gate voltage ($1\ V$ or $-\ 1\ V$). The traditional FET sensor has almost no linear relationship between the signal and the DNA concentration in same condition, as demonstrated in Fig. 4k. The high change intensity, sensitivity and linearity of the signal for gradient DNA concentration suggests that $I_{photocurrent(gate)} + I_{photocurrent(DNA)}$ is sufficient to make traditional FET successfully detect the DNA with ultra-low concentration and is high promising to provide inspiration for other DNA biosensor.

3.4. The roles of DNA and gate voltage in generating photocurrent

The gating effect-dependent band profile of graphene on channel and gating effect-independent band profile of graphene on electrodes is proposed to explain the different photocurrents generated under a sweep gate voltage. Changes of gate-introduced n cause a shifting of the Fermi level for graphene on the channel, based on Equation (1).

The band profile model of the photocurrent-modulated FET sensor was divided into three segments to explain this mechanism, as shown in Fig. 5. Segment A: Gating effect-independent region,

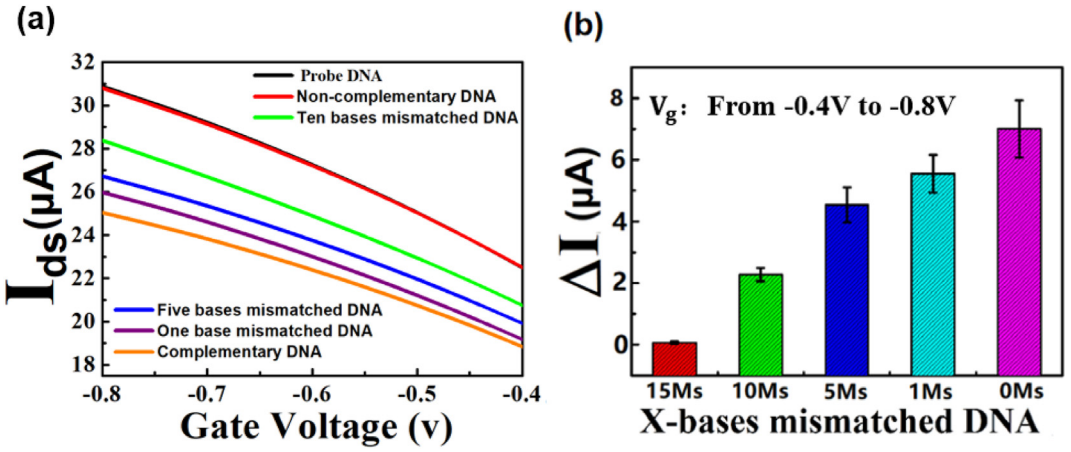

Fig. 6. (a) Part of transfer characteristics of such a biosensor reacted with 100 pM non-complementary DNA, 100 pM one-base mismatched DNA, 100 pM five-base mismatched DNA, 100 pM ten-base mismatched DNA and 100 pM complementary DNA, respectively. (b) The response comparison of the graphene FET biosensor among 100 pM non-complementary DNA, 100 pM ten-bases mismatched DNA, 100 pM five-bases mismatched DNA, 100 pM one-base mismatched DNA and 100 pM complementary DNA.$\Delta I = \left|I_{probe} - I_{X-bases\ mismatched\ DNA}\right|$.

where there is no gate voltage and no bound DNA. There is no gating effect to contribute n to graphene, causing the Fermi level to be fixed. Segment C: Gating effect-dependent region, there is gate voltage and negative charged DNA. Gate-introduced n will modulate the carrier density *N*, as well as the Fermi level. Segment B: transition region, transition region, where the Fermi level of graphene on the electrodes is not equal to the Fermi level of graphene on the channel, forming the band-bending region which can separate the photo-induced carriers to generate photocurrent [34]. The red dashed line presents the Fermi level, the solid colorful lines represent the energy at the charge neutrality point (CNP) and the heavy blue solid line represents graphene. In order to clearly distinguish the carrier density *N* and the energy at charge neutrality point of graphene on the electrodes from that of graphene on the channel, the *N* of graphene in segment A was labeled N_A, the *N* of graphene in segment C was labeled N_C, the energy at charge neutrality point in segment A was labeled E^A_{CNP} and the energy at charge neutrality point in segment C was labeled E^C_{CNP}.

First, the evolution mechanism of photocurrent at $V_g = 0V$ was analyzed in Fig. 5a. Negative charged DNA caused P doping to N type graphene, causing $N_A > N_C$ and E^C_{CNP} moved close to Fermi level in segment C. Thus, E^A_{CNP} is lower than E^C_{CNP}, which form the energy barrier to separate photogenerated carrier and thus generate the photocurrent under the action of the external electric field ($V_{SD} = 0.1\ V$). $E^C_{CNP} \neq E^A_{CNP}$ explains why the photocurrent is not the minimum at $V_g = 0V$ in Fig. 2d.

Next, the evolution mechanism of photocurrent when gate voltage moves in the negative direction was analyzed in Fig. 5b. As shown in process 1, 2, and 3, the E^C_{CNP} moves closer to the Fermi level and then moves above it. Higher negative gate voltage increased the P doping to the *N*-type graphene, causing $E^A_{CNP}$is getting lower and lower than E^C_{CNP}. The change process from $E^C_{CNP2}$to E^C_{CNP3} suggests that the graphene in condition C has changed from N type to P type. During this process, the energy barrier has increased, and that explains why the photocurrent in Fig. 2d increases at more negative gate voltages.

Then, the evolution mechanism of photocurrent was analyzed when gate voltage was moving in the positive direction in Fig. 5c. As shown in process 1, 2, and 3, N_C increases and E^C_{CNP} moves away from the Fermi level, because the increasing positive gate voltage continuously produces N doping to N type graphene. Due to the increasing N doping and electron density, the relationship between $E^A_{CNP}$and E^C_{CNP} changes from $E^A_{CNP} < E^C_{CNP}$ to $E^A_{CNP} > E^C_{CNP}$. This switch explains why the photocurrent in Fig. 2d initially decreased and then increased in the positive gate voltage direction.

Finally, the gradient DNA concentration contributes n to modulate N_C and Fermi level, which suggest DNA with different concentrations can modulate photocurrent to different degree upon sweeping the gate voltage.

3.5. Specificity of the photocurrent-modulated FET sensor

100pM non-complementary DNA (NCDNA), 100 pM one-base mismatched DNA, 100 pM five-base mismatched DNA, 100 pM ten-base mismatched DNA and 100pM fully complementary DNA (FCDNA) were respectively reacted with probe DNA to obtain the specificity of such a photocurrent-modulated FET sensor. As shown in Fig. 6a and Fig. 6b, the red line almost coincides with the black line and the ΔI of non-complementary DNA was found to be negligible, which demonstrated that NCDNA cause very little nonspecific adsorption to graphene and that probe DNA can be bound hard on the surface of graphene by PBASE even after the sensor was rinsed several times by PBS buffer. As the number of base mismatch decreases, complementary DNA signals with different base mismatch degrees are gradually recognized, and the value of ΔI getting larger and larger. In additional, the experiment of Non-target DNA for proving specificity was performed in Fig. S1, where there is almost no signal change before and after the addition of PBS (Non-target DNA). It is clear that the developed biosensor has high specificity for DNA detection.

4. Conclusions

In this study, photocurrent was introduced to modulate the sensitivity of traditional FET for DNA hybridization detection. The response signal:

$$I_{current} + I_{photocurrent(gate)} + I_{photocurrent(DNA)}$$

Make the proposed FET sensor more sensitive for the detection of DNA hybridization as compared to the traditional FET sensors. A sensing mechanism was proposed to explain the reason that DNA with ultra-low concentration was successfully detected under the

specified gate voltage range ($\pm 0.5V$ *to* $\pm 1V$). The developed photocurrent-modulated FET sensor possesses good analytical performance, high current response and good specificity. Improved DNA sensitivity (LOD near 1 aM) was obtained, which is at least 100 times lower than present FET sensors. In the future, the effect of light power to photo-induced responses will be explored experimentally and theoretically to further enhance the sensitivity of traditional FET sensor for DNA hybridization detection. With this initial study, the results strongly suggest that the proposed system holds great promise in ultra-low concentration biosensing and the field of photoelectric analysis.

CRediT authorship contribution statement

Yang Sun: The innovation idea was proposed by, The fabrication and test of this sensor was performed by, The manuscript and figures were finished by, Writing – original draft. **Shicai Xu:** further optimize the experimental plan, VASP simulation was provided by, Writing – original draft. **Tiying Zhu:** VASP simulation was provided by, Writing – original draft. **Jiajun Lu:** VASP simulation was provided by, Writing – original draft. **Shuo Chen:** provided the CVD graphene, Writing – original draft. **Maomao Liu:** The fabrication and test of this sensor was performed by, Writing – original draft. **Guangcan Wang:** provided the CVD graphene, Writing – original draft. **Baoyuan Man:** further optimize the experimental plan, VASP simulation was provided by, Writing – original draft. **Huamin Li:** further optimize the experimental plan, VASP simulation was provided by, Writing – original draft. **Cheng Yang:** The innovation idea was proposed by, The manuscript and figures were finished by, Writing – original draft.

Declaration of competing interest

The authors declare that they have no known competing financial interests or personal relationships that could have appeared to influence the work reported in this paper.

Acknowledgment

This work was supported by National Natural Science Foundation of China (11874244, 11974222); Key Research and development plan of Shandong Province (No. 2019GGX102048); Taishan Scholars Program of Shandong Province (tsqn201812104); Qingchuang Science and Technology Plan of Shandong Province (2019KJJ017).

Appendix A. Supplementary data

Supplementary data to this article can be found online at https://doi.org/10.1016/j.carbon.2021.06.003.

References

[1] T.A. Blauwkamp, S. Thair, M.J. Rosen, L. Blair, M.S. Lindner, I.D. Vilfan, T. Kawli, F.C. Christians, S. Venkatasubrahmanyam, G.D. Wall, Analytical and clinical validation of a microbial cell-free DNA sequencing test for infectious disease, Nature microbiology 4 (4) (2019) 663–674.
[2] J.C. Dudley, J. Schroers-Martin, D.V. Lazzareschi, W.Y. Shi, S.B. Chen, M.S. Esfahani, D. Trivedi, J.J. Chabon, A.A. Chaudhuri, H. Stehr, Detection and surveillance of bladder cancer using urine tumor DNA, Canc. Discov. 9 (4) (2019) 500–509.
[3] F. Barany, Genetic disease detection and DNA amplification using cloned thermostable ligase, Proc. Natl. Acad. Sci. Unit. States Am. 88 (1) (1991) 189–193.
[4] A.M. Aravanis, M. Lee, R.D. Klausner, Next-generation sequencing of circulating tumor DNA for early cancer detection, Cell 168 (4) (2017) 571–574.
[5] M.T. Hwang, M. Heiranian, Y. Kim, S. You, J. Leem, A. Taqieddin, V. Faramarzi, Y. Jing, I. Park, A.M. Van Der Zande, Ultrasensitive detection of nucleic acids using deformed graphene channel field effect biosensors, Nat. Commun. 11 (1) (2020) 1–11.
[6] E.O. Blair, D.K. Corrigan, A review of microfabricated electrochemical biosensors for DNA detection, Biosens. Bioelectron. 134 (2019) 57–67.
[7] M. Kukkar, G.C. Mohanta, S.K. Tuteja, P. Kumar, A.S. Bhadwal, P. Samaddar, K.-H. Kim, A. Deep, A comprehensive review on nano-molybdenum disulfide/DNA interfaces as emerging biosensing platforms, Biosens. Bioelectron. 107 (2018) 244–258.
[8] R. Huang, N. He, Z. Li, Recent progresses in DNA nanostructure-based biosensors for detection of tumor markers, Biosens. Bioelectron. 109 (2018) 27–34.
[9] D. Sarkar, W. Liu, X. Xie, A.C. Anselmo, S. Mitragotri, K. Banerjee, MoS2 field-effect transistor for next-generation label-free biosensors, ACS Nano 8 (4) (2014) 3992–4003.
[10] A. Bonanni, C.K. Chua, G. Zhao, Z.k. Sofer, M. Pumera, Inherently electroactive graphene oxide nanoplatelets as labels for single nucleotide polymorphism detection, ACS Nano 6 (10) (2012) 8546–8551.
[11] J. Liu, X. Chen, Q. Wang, M. Xiao, D. Zhong, W. Sun, G. Zhang, Z. Zhang, Ultrasensitive monolayer MoS2 field-effect transistor based DNA sensors for screening of down syndrome, Nano Lett. 19 (3) (2019) 1437–1444.
[12] S. Xu, J. Zhan, B. Man, S. Jiang, W. Yue, S. Gao, C. Guo, H. Liu, Z. Li, J. Wang, Real-time reliable determination of binding kinetics of DNA hybridization using a multi-channel graphene biosensor, Nat. Commun. 8 (2017) 14902.
[13] M.T. Hwang, Z. Wang, J. Ping, D.K. Ban, Z.C. Shiah, L. Antonschmidt, J. Lee, Y. Liu, A.G. Karkisaval, A.T.C. Johnson, DNA nanotweezers and graphene transistor enable label-free genotyping, Adv. Mater. 30 (34) (2018), 1802440.
[14] B. Cai, S. Wang, L. Huang, Y. Ning, Z. Zhang, G.-J. Zhang, Ultrasensitive label-free detection of PNA–DNA hybridization by reduced graphene oxide field-effect transistor biosensor, ACS Nano 8 (3) (2014) 2632–2638.
[15] Z. Gao, H. Xia, J. Zauberman, M. Tomaiuolo, J. Ping, Q. Zhang, P. Ducos, H. Ye, S. Wang, X. Yang, Detection of sub-fM DNA with target recycling and self-assembly amplification on graphene field-effect biosensors, Nano Lett. 18 (6) (2018) 3509–3515.
[16] J. Mei, Y.-T. Li, H. Zhang, M.-M. Xiao, Y. Ning, Z.-Y. Zhang, G.-J. Zhang, Molybdenum disulfide field-effect transistor biosensor for ultrasensitive detection of DNA by employing morpholino as probe, Biosens. Bioelectron. 110 (2018) 71–77.
[17] Z. Yin, Q. He, X. Huang, J. Zhang, S. Wu, P. Chen, G. Lu, Q. Zhang, Q. Yan, H. Zhang, Real-time DNA detection using Pt nanoparticle-decorated reduced graphene oxide field-effect transistors, Nanoscale 4 (1) (2012) 293–297.
[18] R. Stine, J.T. Robinson, P.E. Sheehan, C.R. Tamanaha, Real-time DNA detection using reduced graphene oxide field effect transistors, Adv. Mater. 22 (46) (2010) 5297–5300.
[19] W. Fu, L. Jiang, E.P. van Geest, L.M. Lima, G.F. Schneider, Sensing at the surface of graphene field-effect transistors, Adv. Mater. 29 (6) (2017), 1603610.
[20] M. Kaisti, Detection principles of biological and chemical FET sensors, Biosens. Bioelectron. 98 (2017) 437–448.
[21] G. Xu, J. Abbott, L. Qin, K.Y. Yeung, Y. Song, H. Yoon, J. Kong, D. Ham, Electrophoretic and field-effect graphene for all-electrical DNA array technology, Nat. Commun. 5 (1) (2014) 1–9.
[22] N. Dontschuk, A. Stacey, A. Tadich, K.J. Rietwyk, A. Schenk, M.T. Edmonds, O. Shimoni, C.I. Pakes, S. Prawer, J. Cervenka, A graphene field-effect transistor as a molecule-specific probe of DNA nucleobases, Nat. Commun. 6 (2015) 6563.
[23] S. Xu, S. Jiang, C. Zhang, W. Yue, Y. Zou, G. Wang, H. Liu, X. Zhang, M. Li, Z. Zhu, Ultrasensitive label-free detection of DNA hybridization by sapphire-based graphene field-effect transistor biosensor, Appl. Surf. Sci. 427 (2018) 1114–1119.
[24] C. Zheng, L. Huang, H. Zhang, Z. Sun, Z. Zhang, G.-J. Zhang, Fabrication of ultrasensitive field-effect transistor DNA biosensors by a directional transfer technique based on CVD-grown graphene, ACS Appl. Mater. Interfaces 7 (31) (2015) 16953–16959.
[25] Y. Sun, Z. Peng, H. Li, Z. Wang, Y. Mu, G. Zhang, S. Chen, S. Liu, G. Wang, C. Liu, Suspended CNT-Based FET sensor for ultrasensitive and label-free detection of DNA hybridization, Biosens. Bioelectron. 137 (2019) 255–262.
[26] J.P. Perdew, K. Burke, M. Ernzerhof, Generalized gradient approximation made simple, Phys. Rev. Lett. 77 (18) (1996) 3865.
[27] A. Batschauer, A plant gene for photolyase: an enzyme catalyzing the repair of UV-light-induced DNA damage, Plant J. 4 (4) (1993) 705–709.
[28] M.H. Patrick, Studies on thymine-derived UV photoproducts in DNA—I. Formation and biological role of pyrimidine adducts in DNA, Photochem. Photobiol. 25 (4) (1977) 357–372.
[29] X. Li, W. Cai, J. An, S. Kim, J. Nah, D. Yang, R. Piner, A. Velamakanni, I. Jung, E. Tutuc, Large-area synthesis of high-quality and uniform graphene films on copper foils, science 324 (5932) (2009) 1312–1314.
[30] Y. Zhang, H. Zheng, Q. Wang, C. Cong, L. Hu, P. Tian, R. Liu, S.L. Zhang, Z.J. Qiu,

Competing mechanisms for photocurrent induced at the monolayer–multilayer graphene junction, Small 14 (24) (2018) 1800691.
[31] M. Jung, P. Rickhaus, S. Zihlmann, P. Makk, C. Schonenberger, Microwave photodetection in an ultraclean suspended bilayer graphene p–n junction, Nano Lett. 16 (11) (2016) 6988–6993.
[32] Y. Yang, J. Li, S. Choi, S. Jeon, J.H. Cho, B.H. Lee, S. Lee, High-responsivity PtSe2 photodetector enhanced by photogating effect, Appl. Phys. Lett. 118 (1) (2021), 013103.
[33] D.-W. Lee, J. Lee, I.Y. Sohn, B.-Y. Kim, Y.M. Son, H. Bark, J. Jung, M. Choi, T.H. Kim, C. Lee, Field-effect transistor with a chemically synthesized MoS 2 sensing channel for label-free and highly sensitive electrical detection of DNA hybridization, Nano Research 8 (7) (2015) 2340–2350.
[34] F. Xia, T. Mueller, R. Golizadeh-Mojarad, M. Freitag, Y.-m. Lin, J. Tsang, V. Perebeinos, P. Avouris, Photocurrent imaging and efficient photon detection in a graphene transistor, Nano Lett. 9 (3) (2009) 1039–1044.